



# FeOOH nanospheres decorated bimetallic NiFe-MOF as efficient dual-functional catalyst towards superior electrocatalytic performance

Yuyang Hu<sup>1</sup>, Yajun Ji<sup>1,\*</sup> , Fuyong Ren<sup>1</sup>, Shufen Tan<sup>1</sup>, and Junnan Yao<sup>1</sup>

<sup>1</sup> School of Materials and Chemistry, University of Shanghai for Science and Technology, Jungong Road 334#, Shanghai 200093, China

Received: 27 June 2022

Accepted: 14 September 2022

Published online:

29 September 2022

© The Author(s), under exclusive licence to Springer Science+Business Media, LLC, part of Springer Nature 2022

## ABSTRACT

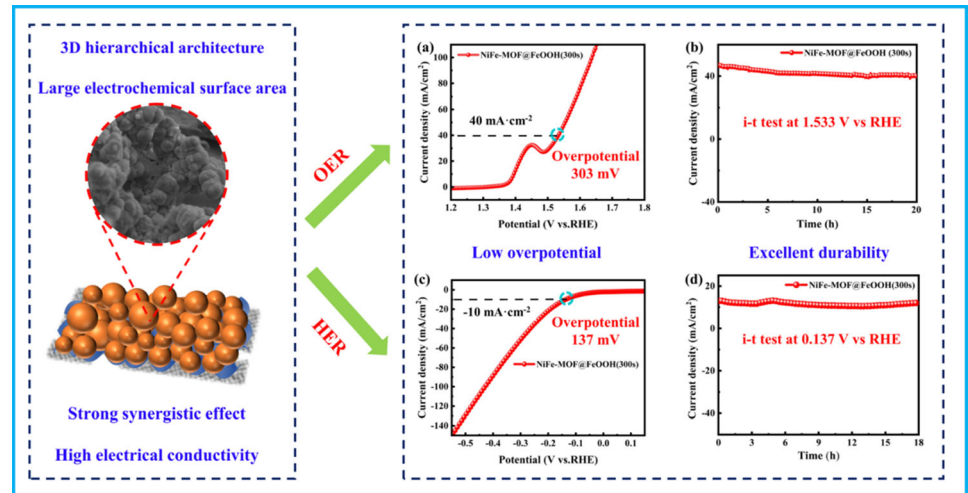
Exploring dual-functional metal-based hydrogen evolution reaction (HER) and oxygen evolution reaction (OER) electrocatalyst with high activity and stability is an indispensable strategy to effectively utilize hydrogen energy and alleviate energy crisis. Herein, a series of dual-functional NiFe-MOF@FeOOH-based composites with different electrodeposition intervals were synthesized via a solvothermal method and subsequent electrodeposition process. It was noted that when the electrodeposition time was set as 300 s, the corresponding composites exhibited the most effective OER catalytic activity with a low overpotential of 303 mV at 40 mA cm<sup>-2</sup>. The optimal composites also displayed fast reaction kinetics with a small tafel plot of 36 mV dec<sup>-1</sup> and superior durability for 20 h. Meanwhile, the composite only required 137 mV for HER to reach a catalytic current density of 10 mA cm<sup>-2</sup> under the same condition. Clearly, the obtained composites depicted excellent dual-functional electrocatalytic performance which can be ascribed to its unique 3D hierarchical structure, larger electrochemical surface area, strong synergistic effect as well as improved electrical conductivity. Besides, the adopted FeOOH was favorable for the transformation from Ni<sup>2+</sup> to Ni<sup>3+</sup>, which acted as the active centers of catalytic reaction to advance the OER process. All in all, this study provided a novel insight to design bimetallic MOF based electrode materials with both excellent HER and OER properties.

Handling Editor: Catalin Croitoru.

Address correspondence to E-mail: jiyajun@usst.edu.cn

<https://doi.org/10.1007/s10853-022-07748-x>

## GRAPHICAL ABSTRACT



## Introduction

Nowadays, serious energy crisis and dramatic environment pollution caused by aggressive fossil fuel depletion arose widespread public concern [1, 2]. To tackle the issue above, electrochemical water splitting has been demonstrated as one of the most promising methods for large-scale production of clean hydrogen and oxygen, which is conducive to alleviating energy crisis and environmental pollution. Generally, it refers to HER at the cathode and OER at the anode [3]. However, the lethargic kinetics of the two crucial half-reactions result in low water splitting efficiency, which required much higher decomposition voltage than the theoretical voltage ( $1.23 \text{ V}$ ) [4]. At present, although traditional precious metal-based electrocatalysts such as Pt [5], Ir [6] and Ru [7] had shown effective behaviors for HER or OER, their high cost, scarce resources and extraction difficulty greatly limited their large-scale application [8]. Thus, it is highly desirable to exploit low-cost and high-performance bifunctional electrocatalysts to reduce the large overpotential and eventually to improve water decomposition efficiency [9, 10].

Recently, a large number of transition metal-based catalysts (such as transition metal phosphates [11], sulfides [12], carbides [13], hydroxides [14], etc.) have

been explored in depth for the preparation of HER and OER dual-functional materials to replace expensive rare Pt-based HER and Ir-based OER catalysts. Especially, transition metal–organic frameworks (MOFs) have stimulated huge attentions and are considered as one of the optimal precursors for efficient HER and OER electrocatalysts benefiting from their high porosity and adjustable specific surface area [15–17]. In contrast to single-metal MOFs, bimetallic MOFs were proved to exhibit stronger coupling effect and became the current research hotspot [18]. Among various bimetallic MOFs, Fe/Ni bimetallic MOFs displayed state-of-the-art catalytic performance and the most extensive application prospect by virtue of high specific surface area, significant structural complexity and flexible characters with versatile coordination chemistry of metal cations [19]. For instance, Sun et al. synthesized 3D bimetal MIL-53(FeNi)/NF with extraordinary OER of  $233 \text{ mV}$  to reach  $50 \text{ mA} \cdot \text{cm}^{-2}$ ,  $76 \text{ mV}$  lower than single-metal Ni-MOFs. The introduction of Fe was demonstrated effectively to increase the electrochemical active region [20]. Then, NiFe-MOF-74 was prepared by Xing et al. as an OER electrocatalyst with an overpotential of  $223 \text{ mV}$  at  $10 \text{ mA} \cdot \text{cm}^{-2}$ . The advanced performance was attributed to the synergistic effect of Ni and Fe [21]. Thereafter, Chen et al. synthesized two-dimensional NiFe-MOF-74 nanosheets, which

exhibited fascinating bifunctional performance with a lower overpotential 208 mV for OER, 195 mV for HER and 1.58 V for overall water splitting at 10 mA cm<sup>-2</sup> [22]. Although bimetallic Fe/Ni MOFs had made some progress, the relatively low conductivity and poor stability in alkaline solutions severely hampered their further applications [23, 24].

In order to address these problems mentioned above, diverse strategies including the adoption of different conductive substrates [25, 26], doping engineering [27, 28] as well as coupling [29] had been applied. Notably, combining NiFe-MOF with other functional materials to form active MOF composites was deemed as a more promising method to improve their inherent electrocatalytic activity [30]. For example, Li et al. prepared NiFe MOF/OM-NFH composite by in-situ growth method. The resulted composite demonstrated outstanding OER activity with a small overpotential of 270 mV at 10 mA cm<sup>-2</sup>, which can be derived from the more exposed NiFe active centers and the improved electron transfer rate [31]. Then, rGO@Fe<sub>2</sub>Ni MIL-88(1:1) composite was fabricated by Reza Abazari with remarkable OER performance: to drive 10 mA cm<sup>-2</sup>, its overpotentials were only 264 mV. Moreover, FeNi Mil-88(1:1) was uniformly deposited on the surface of the rGO nanosheets, which effectively prevented the agglomeration of rGO nanosheets and enhanced the accessibility of catalyst surfaces for the aqueous electrolyte [32]. Additionally, An et al. constructed the composite CeO<sub>2</sub>@NiFe-MOF by coordinating CeO<sub>2</sub> with NiFe-MOF. NiFe-MOFs were nonuniformly distributed on the surface of CeO<sub>2</sub> nanosheets, which exposed more active sites and significantly enhanced the OER activity [33]. All these researches above can clearly prove that coupling NiFe-MOF with other functional materials can effectively boost the catalytic properties. Recently, FeOOH is considered to be a promising electrocatalyst for OER due to its strong adsorption of hydroxyl species, low cost, natural abundance, and environmental friendliness [34, 35]. For instance, Li et al. reported the strong synergistic effect between FeOOH and NiCo<sub>2</sub>O<sub>4</sub> could ensure efficient electron interaction at the interface of NiCo<sub>2</sub>O<sub>4</sub>@FeOOH and high charge transfer rate, which induced the composite to display marvelous HER and OER activity [36]. After that, from Chen's report, the oxidation of Ni<sup>2+</sup> in the Ni-Fe LDH could be promoted effectively by the highly oxidative interfacial Fe<sup>(3+δ)+</sup> species from the

defective FeOOH NPs, resulting in greatly enhanced OER performance [37]. Moreover, Liang et al. elaborated that the strong electron interaction between FeOOH and NiFe-LDH from the stable FeOOH/NiFe-LDH heterostructure profoundly promoted the OER activity [38]. Nevertheless, to our best of knowledge, there are no reports about the combining FeOOH with NiFe-MOF to construct NiFe-MOF@FeOOH composites and their corresponding HER and OER performance.

Inspired by the aforementioned considerations, in this work, a series of 3D NiFe-MOF@FeOOH bifunctional catalysts were constructed on nickel foam (NF) via a solvothermal method and subsequent electrodeposition process. The effect of various electrodeposition intervals on the electrocatalytic performance was systematically investigated. Thanks to the existence of a synergistic effect between NiFe-MOF and FeOOH, the optimal sample illustrated an excellent dual-functional activity with small overpotentials both for OER and HER and maintained remarkable stability. Furthermore, the intrinsic reasons for the superior HER and OER performance were discussed.

## Experimental section

### Materials and reagents

All reagents utilized are listed as follows: Nickel nitrate hexahydrate (Ni(NO<sub>3</sub>)<sub>2</sub>·6H<sub>2</sub>O), iron nitrate nonahydrate (Fe(NO<sub>3</sub>)<sub>3</sub>·9H<sub>2</sub>O), 1,3,5-triformic acid(H<sub>3</sub>BTC), N,N-dimethylformamide (DMF), potassium hydroxide (KOH), ethanol (C<sub>2</sub>H<sub>6</sub>O). The reagents are analytical-grade and used without further purification.

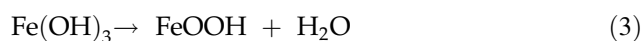
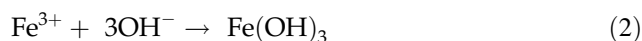
### Synthesis of leaves-like bimetal NiFe-MOF on NF

In this work, leaves-like NiFe-MOF nanosheets were grown on NF via one-step solvothermal route. The specific steps are as follows: Firstly, a piece of NF(2 cm × 3 cm) was cleaned through immersing in 40 ml ethanol under ultra-sonication for 30 min, then cleaned for several times with deionized water and ethanol. Then, 1 mmol Ni(NO<sub>3</sub>)<sub>2</sub>·6H<sub>2</sub>O and 1 mmol Fe(NO<sub>3</sub>)<sub>3</sub>·9H<sub>2</sub>O were dispersed to 40 ml absolute alcohol, which was called the solution A. Meanwhile,

1 mmol H<sub>3</sub>BTC was dispersed into 10 ml DMF, which was named as the solution B. Thereafter, the solution B was poured slowly into the solution A, which was stirred at 550 rev min<sup>-1</sup> continuously for 30 min to form a clear brown-yellow solution. Subsequently, the brown-yellow solution and one piece of treated NF were transferred to a 100 ml Teflon-lined high-pressure stainless-steel autoclave and heated at 150 °C for 12 h. After the autoclave was cooled down to room temperature naturally, the resulted NF was taken out and washed with deionized water and ethanol for several times, and dried at 60 °C for 12 h. The obtained material was labeled as NiFe-MOF.

### Preparation of NiFe-MOF@FeOOH nanocomposites

FeOOH was further electrodeposited on the surface of NiFe-MOF in a typical three-electrode system, where the NiFe-MOF was regarded as a working electrode and platinum wire and KCl-saturated Ag/AgCl were used as the counter electrode and reference electrode, respectively. The electrolyte solution consists of dissolving 1 mmol Fe(NO<sub>3</sub>)<sub>3</sub>·9H<sub>2</sub>O and 1 mmol Na<sub>2</sub>SO<sub>4</sub> in 50 ml water. Amperometric I-T curve was used for electrodeposition at a deposition potential of -1.0 V at room temperature. After electrodeposition, the obtained products were carefully cleaned with water and anhydrous ethanol, eventually dried in a vacuum furnace at 60 °C for 12 h. In order to study the effect of different electrodeposition intervals on the electrocatalytic performance, the electrodeposition time was set as 100 s, 300 s and 500 s, and the corresponding samples were named as NiFe-MOF@FeOOH(100 s), NiFe-MOF@FeOOH(300 s) and NiFe-MOF@FeOOH(500 s), respectively. For comparison, the pristine FeOOH on NF under the same condition was prepared, which was labeled as FeOOH. Since the accumulation of OH<sup>-</sup> in local areas could lead to the deposition of FeOOH, the possible formation of FeOOH during the electrodeposition process can be expressed by the following formulas [36]



### Characterization

The morphology and microstructure of the catalysts were observed by scanning electron microscopy (SEM; Thermo VEG 3 TESCAN). Transmission electron microscopy (TEM, FEI Tecnai G2 F20 S-Twin) was obtained to further explore the internal structure of the material under 200 kV voltage. X-ray diffraction (XRD) was applied to study the crystallization catalyst properties and the composition and types of the synthesized crystal materials at an accelerating voltage of 40 kV and a current of 40 mA. X-ray photoelectron spectroscopy (XPS, EscaLab 250 Xi) was conducted to analyze the chemical bonds and elemental valence states of the active materials.

### Electrochemical test of materials

The electrochemical tests of the catalysts were carried out in a three-electrode system using a CHI 660E electrochemical workstation analyzer with 1 M KOH as the electrolyte. The standard Ag/AgCl electrode was utilized as the reference electrode, the Pt wire served as the counter electrode, and the prepared NiFe-MOF@FeOOH was used as the working electrode. Electrochemical tests such as linear sweep voltammetry (LSV), electrochemical impedance (EIS), chronoamperometry test (i-t) and cyclic voltammetry (CV) were performed on the synthesized samples to explore the activity, conductivity, stability and catalytic efficiency. The charge transfer kinetics of the catalysts were also investigated with the corresponding Tafel slopes derived from LSV curves. Moreover, the double layer capacitance (C<sub>dl</sub>) was measured by CV at different scanning rates in the non-Faraday potential range of -0.10–0 V. All measured potentials were converted to RHE: E<sub>RHE</sub> = E<sub>Ag/AgCl</sub> + 0.059 × pH + 0.197(V). The area of electrode material immersed in KOH electrolyte is about 1 cm<sup>2</sup>.

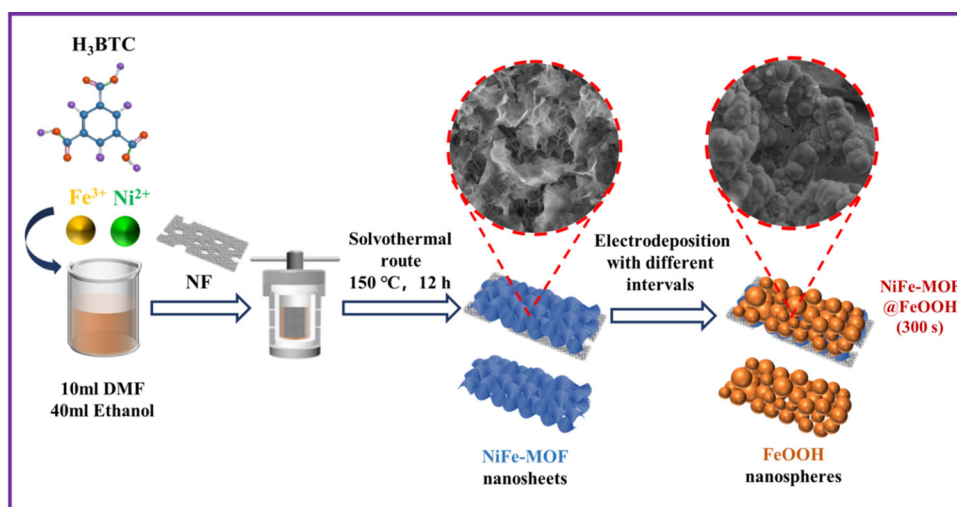
## Results and discussion

### Synthesis and characterization of the electrocatalysts

The procedure for fabricating the NiFe-MOF@FeOOH electrode was vividly depicted in Fig. 1. Initially, the precursor with Ni<sup>2+</sup> and Fe<sup>3+</sup> was



**Figure 1** Flow charts of the synthetic process.



dissolved in mixed solution containing ethanol and homo-triformic acid. Then, a certain amount of DMF and a piece of clean nickel foam were transferred to the above solution and heated at 150 °C for 12 h to form leaf-like NiFe-MOF nanosheets, which was then utilized as the substrate for further modification. Subsequently, FeOOH nanospheres were uniformly grown on the surface of NiFe-MOF nanosheets via a facile one-step electrodeposition route. What is more, the effect of various electrodeposition intervals on the electrochemical performance had been investigated and the optimal electrodeposition time was determined.

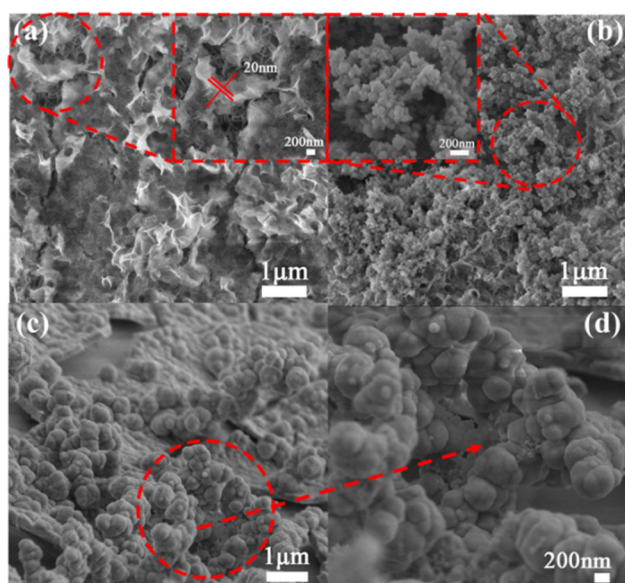
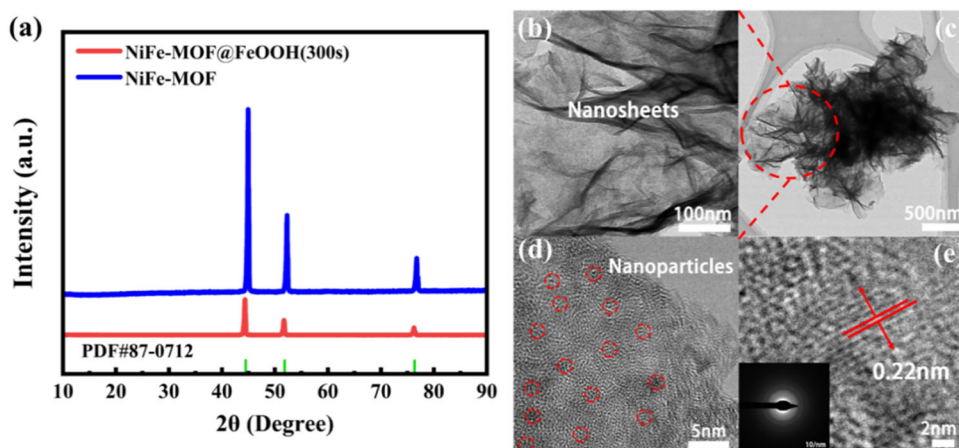


**Figure 2** FE-SEM images of **a** NiFe-MOF **b** pristine FeOOH and **c**, **d** NiFe-MOF@FeOOH(300 s) with different magnifications.

As exhibited in Fig. 2, the surface morphologies of NiFe-MOF, pristine FeOOH and NiFe-MOF@FeOOH(300 s) were characterized by FE-SEM. Figure 2a depicted leaf-like NiFe-MOF nanosheets were crimped and grown on the porous NF. From the high magnification inserted in the upper right corner of Fig. 2a, it can be found that the average thickness of the nanosheets is about 20 nm. Moreover, it can be anticipated that the intertwined formation of multiple small gaps among nanosheets could facilitate the infiltration and mass transfer of electrolyte and provide a large number of active sites for FeOOH attachment thereafter. For comparison, the solely electrodeposited FeOOH on NF via the same electrodeposition procedure is depicted in Fig. 2b. It can be noted that numerous FeOOH nanoparticles with average size about 100 nm were aggregated on the surface of NF. Figure 2c depicted tight growth and stacked high-density spherical FeOOH nanoparticles covering NiFe-MOF nanosheets on a large scale. From a larger magnification(Fig. 2d), it can be observed that the average diameter of the FeOOH nanospheres is approximately 700 nm. Undoubtedly, the FeOOH nanospheres were successfully adopted and attached closely to the surface of the leaf-like NiFe-MOF nanosheets after electrodeposition.

Moreover, the crystallographic structure and phase purity of NiFe-MOF and NiFe-MOF@FeOOH(300 s) were examined by XRD in Fig. 3a. It is notable that there were no other XRD peaks except the Ni foam substrate based characteristic peaks can be observed in the two samples. The absence of corresponding characteristic diffraction peaks can be attributed to the small size and low crystallinity of the resulted

**Figure 3** a XRD patterns of NiFe-MOF and NiFe-MOF@FeOOH(300 s); b, c TEM images of NiFe-MOF@FeOOH(300 s); d, e HRTEM images of NiFe-MOF@FeOOH(300 s) (Inset depicted the corresponding SAED pattern).



materials, which expressed the same tendency as previous reported works [36, 39]. Besides, the microstructure of NiFe-MOF@FeOOH(300 s) was further investigated by TEM and HRTEM. Figure 3c revealed a intertwined and stacked nanosheet morphology and the thickness of the nanosheets focused on 20 nm from the magnified image (Fig. 3b). The observed results were totally consistent with SEM results. From the HRTEM in Fig. 3d, there were multiple tiny nanoparticles decorated on the surface. And it can be obtained from Fig. 3e that the lattice gap is about 0.22 nm, corresponding to the (220) crystal plane of NiFe-MOF [40]. However, there was no obvious lattice fringe referred to FeOOH, indicating its low crystallinity. The corresponding SAED pattern inserted demonstrated the same tendency. The observed relatively low crystallinity of the product from HRTEM characterization was coincident with the XRD analyses referred above.

In order to reveal the specific surface chemical elements composition and valence state of NiFe-MOF@FeOOH(300 s), XPS was proceeded. Obviously, four distinct elements such as Fe, Ni, C and O can be seen in the full spectrum (Fig. 4a). In Fig. 4b, the high resolution XPS spectrum of C 1s can be deconvoluted into three peaks at approximately 288.6 eV, 285.5 eV and 284.7 eV, belonging to the three carboxyl bonds O-C=O, C-O and C-C=C of the aromatic ring of H<sub>3</sub>BTC, respectively [19, 41, 42]. The O 1s XPS spectrum in Fig. 4c simulated the three peaks around 532.2 eV, 531.4 eV and 529.7 eV, which represented O-H, O=C-O and Fe-O, respectively [43]. This may be related to the formed Fe-O-Fe and Fe-O-H bonds, which can preliminarily prove the existence of FeOOH. Figure 4d showed the Fe 2p

nuclear level spectrum. Clearly, it presented two main peaks at Fe 2p<sub>3/2</sub> (711.5 eV) and Fe 2p<sub>1/2</sub> (725.1 eV), accompanied by two satellite peaks at about 718 eV and 733.2 eV, separately. The Fe 2p<sub>1/2</sub> peak could be assigned to two peaks around 724.4 eV and 726 eV representing the presence of Fe<sup>2+</sup> and Fe<sup>3+</sup>, respectively. The Fe 2p<sub>3/2</sub> peak could be divided into two peaks centered at 710.8 eV and 712.4 eV, corresponding to Fe<sup>2+</sup> and Fe<sup>3+</sup>, separately. It can be speculated that Fe<sup>3+</sup> was partially reduced to Fe<sup>2+</sup> [42, 44] during the electrodeposition process. According to previous studies, the existence of Fe<sup>2+</sup> was more favorable for absorption of H<sub>2</sub>O molecule, thus boosting the OER performance activity [45, 46].

The high resolution XPS spectrum of Ni 2p in Fig. 4e displayed the fitting peaks of the two valence states of nickel ion and two satellite peaks. There were two major spin-orbit peaks (Ni 2p<sub>1/2</sub> and Ni 2p<sub>3/2</sub>) besides two shakeup satellite peaks located at 861.8 and 879.5 eV. 855.6 eV (2p<sub>3/2</sub>) and 873.1 eV (2p<sub>1/2</sub>) near the main peak Ni 2p<sub>3/2</sub> can be ascribed to the formation of Ni-O bond, which was assigned to Ni<sup>2+</sup> [47, 48]. 856.3 eV (2p<sub>3/2</sub>) and 873.9 eV (2p<sub>1/2</sub>) near the main peak Ni 2p<sub>1/2</sub> were attributed to the presence of Ni-OH, which indicated the formation of a link-effect between the nickel ion and hydroxyl group in the MOF and also corresponded to high valence of Ni<sup>3+</sup> [49]. The presence of Ni<sup>3+</sup> was beneficial to rapidly induce the deprotonation of OOH species and thereby facilitate the production of oxygen due to its lower coordination number and higher adsorption energy of H<sub>2</sub>O [39]. Meanwhile, a small peak appeared at around 852.6 eV, representing the zero-valent nickel Ni<sup>0</sup> derived from NF [50]. All these

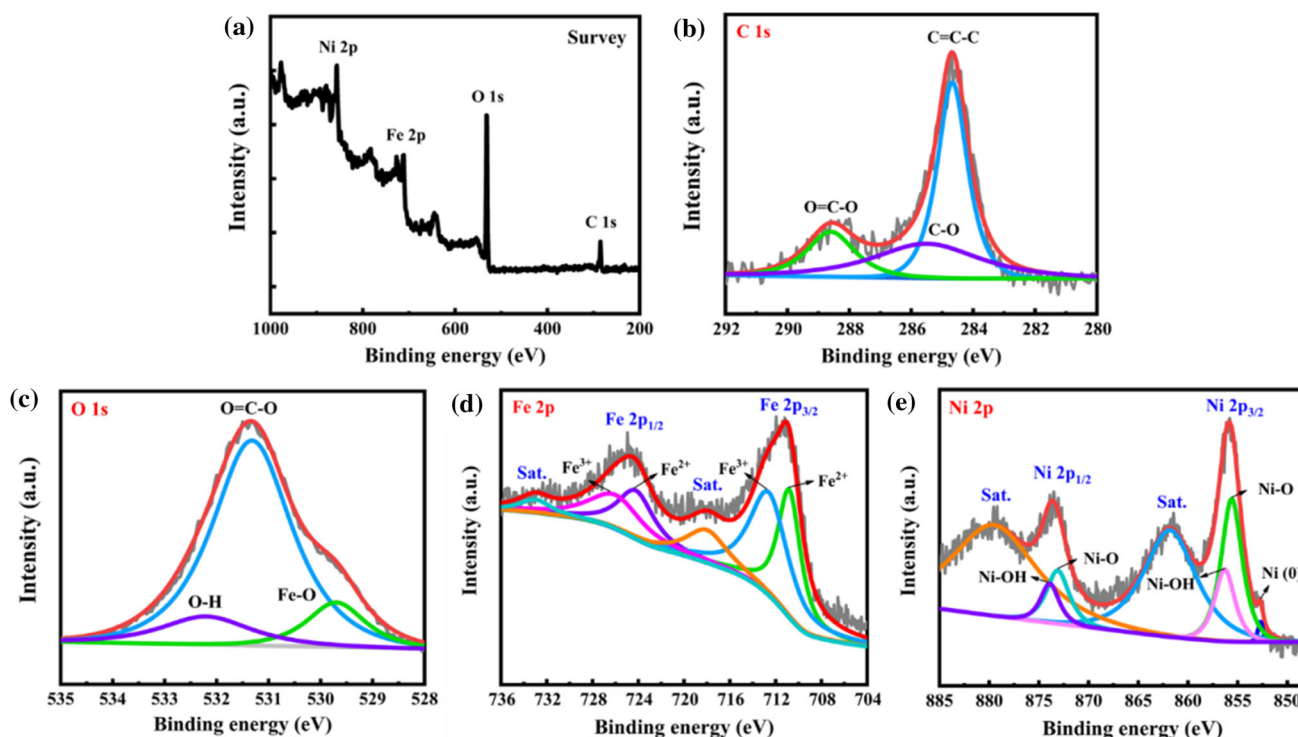


**Figure 4** a XPS full survey spectra of NiFe-MOF@FeOOH(300 s); The detailed XPS spectra of C 1 s (b), O 1 s (c), Fe 2p (d) and Ni 2p (e).

results above confirmed that NiFe-MOF@FeOOH composites had been successfully synthesized.

### OER catalytic activity

In 1 M KOH solution, the OER performance of the obtained catalysts were evaluated by LSV at a scan rate of  $5 \text{ mV s}^{-1}$ . Figure 5a displayed the LSV curves of NiFe-MOF and NiFe-MOF@FeOOH composites with different deposition intervals, and the histogram in Fig. 5b demonstrated the corresponding concrete overpotential values at  $40 \text{ mA cm}^{-2}$ . It can be noted that the NiFe-MOF@FeOOH(300 s) based electrode exhibited remarkable OER activity with the smallest overpotential of 303 mV at a current density of  $40 \text{ mA cm}^{-2}$ , which was much lower than those of NiFe-MOF@FeOOH(100 s)(353.1 mV) and NiFe-MOF@FeOOH(500 s)(374.1 mV). In contrast, NiFe-MOF(441.1 mV) exhibited a fairly high overpotential to afford  $40 \text{ mA cm}^{-2}$ . The insert in Fig. 5a exhibited the OER performance of FeOOH, which expressed a high overpotential of 400.1 mV at  $40 \text{ mA cm}^{-2}$ . It can be verified that the optimal deposition time to achieve the best OER performance for NiFe-MOF@FeOOH is 300 s. From the whole LSV curves, it can be

noted that there were conspicuous oxidation peaks around 1.4 V(vs RHE) for NiFe-MOF, NiFe-MOF@FeOOH(100 s) and NiFe-MOF@FeOOH(300 s). This can be ascribed to the  $\text{Ni}^{2+}/\text{Ni}^{3+}$  transformation to form  $^*\text{OOH}(\text{NiOOH})$ , which can act as active centers for intermediate transformation from  $\text{OOH}^*$  to  $\text{O}_2$  in the catalytic process, and thus showing dramatic OER catalytic performance [51–53]. Moreover, the observed improved OER activity of NiFe-MOF@FeOOH composites compared with NiFe-MOF proved that the electrocatalytic performance of NiFe-MOF could be effectively boosted through depositing with FeOOH. However, since the relatively short deposition time(only 100 s) led to possibly low loading amount and incomplete coating, the improvement of catalytic performance was finite. With further increasing the deposition time to 300 s, the corresponding composite depicted the best OER property. What is more, the  $\text{Ni}^{2+}/\text{Ni}^{3+}$  redox potentials for NiFe-MOF@FeOOH(100 s) and NiFe-MOF@FeOOH(300 s) gradually declined, which demonstrated that the adopted FeOOH could lower and adjust the energy barrier for the conversion of  $\text{Ni}^{2+}$  to  $\text{Ni}^{3+}$  [54, 55]. Nevertheless, when prolonging the deposition time to 500 s, the NiFe-



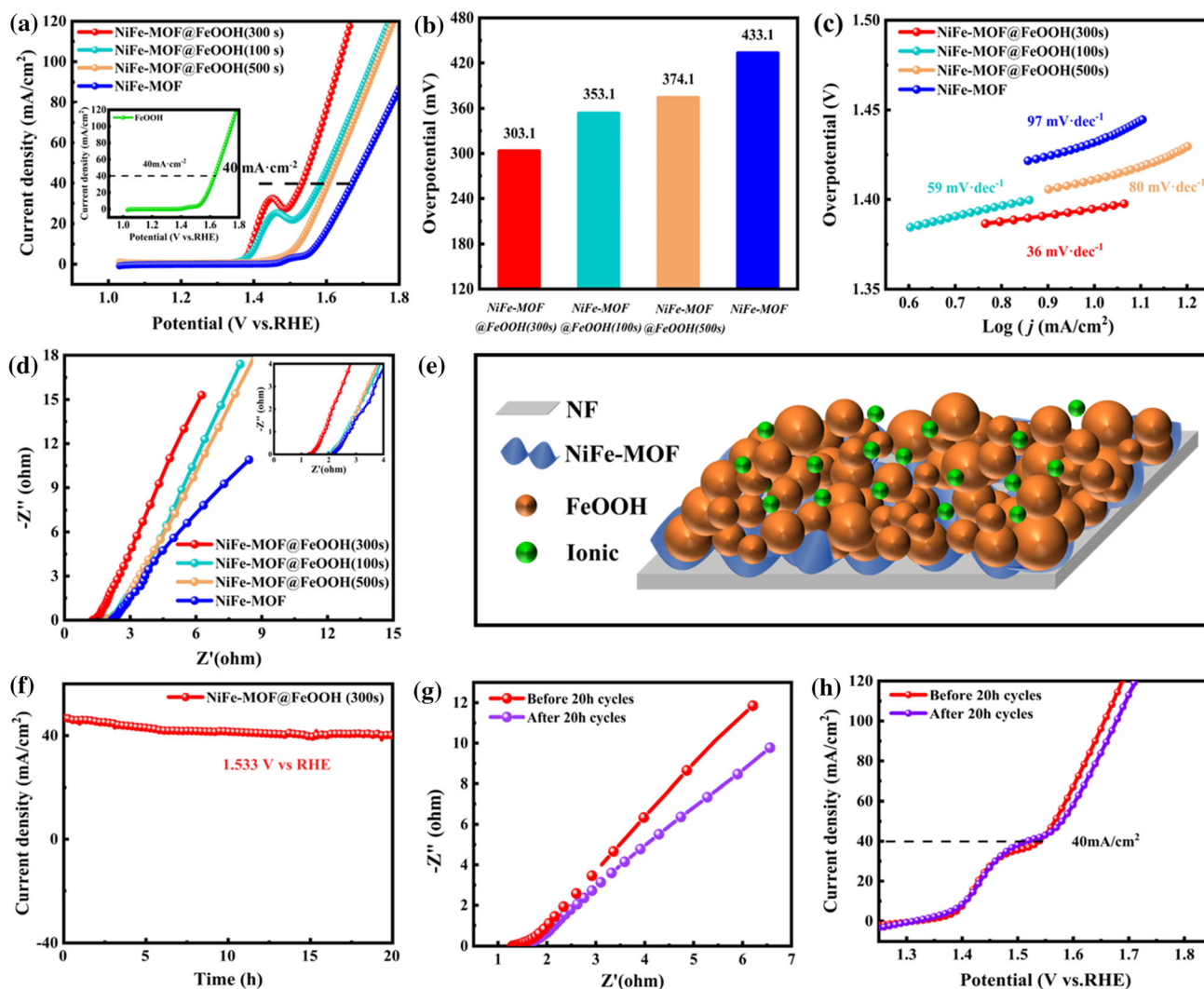


**Figure 5** **a** OER polarization curves of obtained catalysts. The inset exhibited the OER performance of FeOOH; **b** The corresponding overpotential histogram; **c** Tafel plots obtained from the OER curves in Fig. 5 **a**; **d** EIS impedance diagram. The inset showed the magnified image of EIS focused at a high

frequency; **e** Schematic illustration of the unique 3D hierarchical structure of NiFe-MOF@FeOOH(300 s) composites and the possible distribution of ionic among them; **f**) i-t cycle diagram at 1.533 V vs RHE. The EIS diagram (**g**) and LSV curves (**h**) of NiFe-MOF@FeOOH(300 s) before and after 20 h circles.

MOF@FeOOH(500 s) exhibited a deteriorated OER activity, which was close to that of NiFe-MOF. The possible explanation could be attributed to the thick layer of FeOOH on the surface derived from the extended deposition duration would cover the NiFe-MOF substrate totally, which blocked the numerous reactive sites thus degrading the electrocatalytic property [56]. Moreover, the kinetic parameters such as the Tafel slope of the above electrocatalysts [57] were then conducted to explore the constitutive reaction mechanism of OER. As depicted in the Fig. 5c, the Tafel slope of NiFe-MOF@FeOOH(300 s) (36 mV dec<sup>-1</sup>) depicted the

smallest value which was significantly lower than that of NiFe-MOF@FeOOH(100 s) (59 mV dec<sup>-1</sup>), NiFe-MOF@FeOOH(500 s) (80 mV dec<sup>-1</sup>) and NiFe-MOF (97 mV dec<sup>-1</sup>). In general, electrocatalysts with smaller Tafel slopes illustrated faster charge transfer kinetics, which was favorable for accelerating the OER process [58, 59].

Thereafter, the kinetics of the reaction process of the catalysts and the electron transfer rate in the electrolyte were further investigated by EIS in Fig. 5d[60]. Clearly, it can be found that the NiFe-MOF@FeOOH(100 s) exhibited improved conductivity compared with that of pristine NiFe-MOF. When



further increasing the deposition interval to 300 s, the NiFe-MOF@FeOOH(300 s) exhibited the most outstanding conductivity. Conspicuously, the Warburg straight line slope of NiFe-MOF@FeOOH(300 s) was the lowest among all four materials, elucidating that the diffusion resistance of electrons in NiFe-MOF@FeOOH(300 s) was the smallest. Moreover, from the inserted image in Fig. 5d, it was noted that NiFe-MOF@FeOOH(300 s) also illustrated the lowest connection resistance( $R_s$ )(1.2  $\Omega$ ), which was less than that of NiFe-MOF@FeOOH(100 s)(1.9  $\Omega$ ), NiFe-MOF@FeOOH(500 s)(2  $\Omega$ ) and NiFe-MOF(2.1  $\Omega$ ). As vividly depicted in Fig. 5e, the excellent conductivity can be ascribed to the resulted 3D hierarchical structure of NiFe-MOF@FeOOH(300 s) with plentiful crevices could supply fast diffusion channels to guarantee efficient mass transfer of electrolyte to the active centers [61] and the closely intimate contact and possible synergistic effect between NiFe-MOF and FeOOH. There is no doubt that NiFe-MOF decorated with FeOOH can effectively improve the electrical conductivity. Nevertheless, when the deposition time prolonged to 500 s, the corresponding composite illustrated the deteriorated electrical conductivity. The obtained EIS results matched well with the OER tests.

What is more, the stability of NiFe-MOF@FeOOH(300 s) was assessed by performing i-t test at the potential of 1.533 V vs RHE, which is a vital parameter to evaluate the catalytic performance in the practical application [62]. As shown in Fig. 5f, the stable current concentrated at 40 mA cm<sup>-2</sup> even after 20 h continuous operation revealed that the NiFe-MOF@FeOOH(300 s) catalyst exhibited an extraordinary durability for OER. Furthermore, the slightly varied EIS and LSV curves after long-term stability test as depicted in Fig. 5g, h further confirmed the extraordinary durability of the composites.

It had been reported that the double-layer capacitance( $C_{dl}$ ) determined by CV measurements in a non-Faradaic region can be used to calculate the electrochemical surface area (ECSA), as the current produced in this region originated from the charging of the electrical double layer and was proportional to ECSA [42, 63]. Figure 6a, b depicted a series of scan rates(from 20 mV s<sup>-1</sup> to 180 mV s<sup>-1</sup>) with a range of current densities CV curves of NiFe-MOF@FeOOH(300 s) and NiFe-MOF polar materials from -0.10 V to 0.00 V.

A  $C_{dl}$  of 4.52 mF cm<sup>-2</sup> was obtained for NiFe-MOF@FeOOH(300 s), while NiFe-MOF exhibited the lower values of 3.87 mF cm<sup>-2</sup> as shown in Fig. 6c. According to the equation  $ECSA = A \times C_{dl}/C_s$  ( $A$  represents the geometrical working area and  $C_s$  is estimated to be 0.04 mF cm<sup>-2</sup>) [44], the ECSAs for NiFe-MOF@FeOOH(300 s) and NiFe-MOF were estimated to be 113.00 cm<sup>2</sup> and 96.75 cm<sup>2</sup>, respectively(Fig. 6d). Obviously, it can be confirmed that NiFe-MOF@FeOOH(300 s) can offer a larger electrochemical surface area and more catalytic active sites for the energy conversion process than that of NiFe-MOF, the adopted FeOOH can substantially modulate the surface electrochemical properties.

### HER catalytic activity

Furthermore, the HER performance of NiFe-MOF@FeOOH(300 s) was explored. The polarization curves obtained from the LSV test were displayed in Fig. 7a. It can be noted that NiFe-MOF@FeOOH(300 s) achieved the optimal HER catalytic activity under the provided voltage range. Noteworthy, it delivered a current density of 10 mA cm<sup>-2</sup> with only overpotential of 137 mV, which was superior than that of pristine FeOOH(202 mV) as depicted in the inset of Fig. 7a. This catalytic activity was also superior than many recently reported iron- and nickel-based electrocatalysts(as shown in Table 1), which could be ascribed to the heterogeneous structure with strong synergistic effect between NiFe-MOF and FeOOH [35]. Figure 7b displayed the corresponding Tafel slope gained from the LSV curves. Conspicuously, NiFe-MOF@FeOOH(300 s) exhibited a tafel slope of 160 mV dec<sup>-1</sup>. Theoretically, when the Tafel slope is close to 120 mV dec<sup>-1</sup>, 40 mV dec<sup>-1</sup> and 30 mV dec<sup>-1</sup>, the responses follow the Volmer, Volmer-Heyrovsky and Volmer-Tafel mechanisms, respectively [64]. Clearly, since the Tafel slope of NiFe-MOF@FeOOH(300 s) is close to 120 mV dec<sup>-1</sup>, there is no doubt that they follow the Volmer step. To further investigate the charge/ion diffusion properties, the EIS tests were proceed and shown in Fig. 7c. Obviously, the high slope of the Warburg straight line revealed the low diffusion resistance of electrons in NiFe-MOF@FeOOH(300 s), which confirmed that the NiFe-MOF@FeOOH(300 s) electrocatalyst possessed an excellent conductivity.

Additionally, the i-t curve was measured at a potential of 0.137 V vs RHE to further examine the

**Figure 6** CV curves of **a** NiFe-MOF@FeOOH(300 s) and **b** NiFe-MOF at different scan rates (20, 60, 100, 140 and 180  $\text{mV s}^{-1}$ ); **c** corresponding  $C_{dl}$  curves; **d** ECSA histogram.

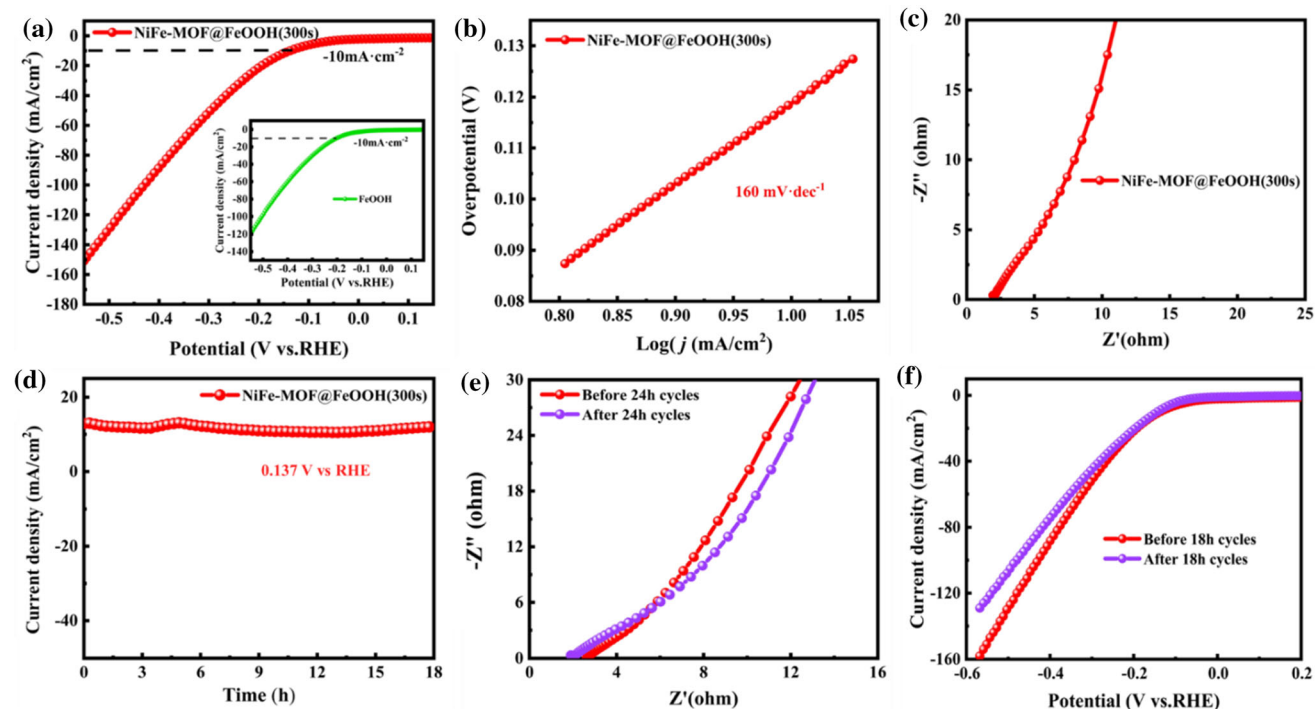
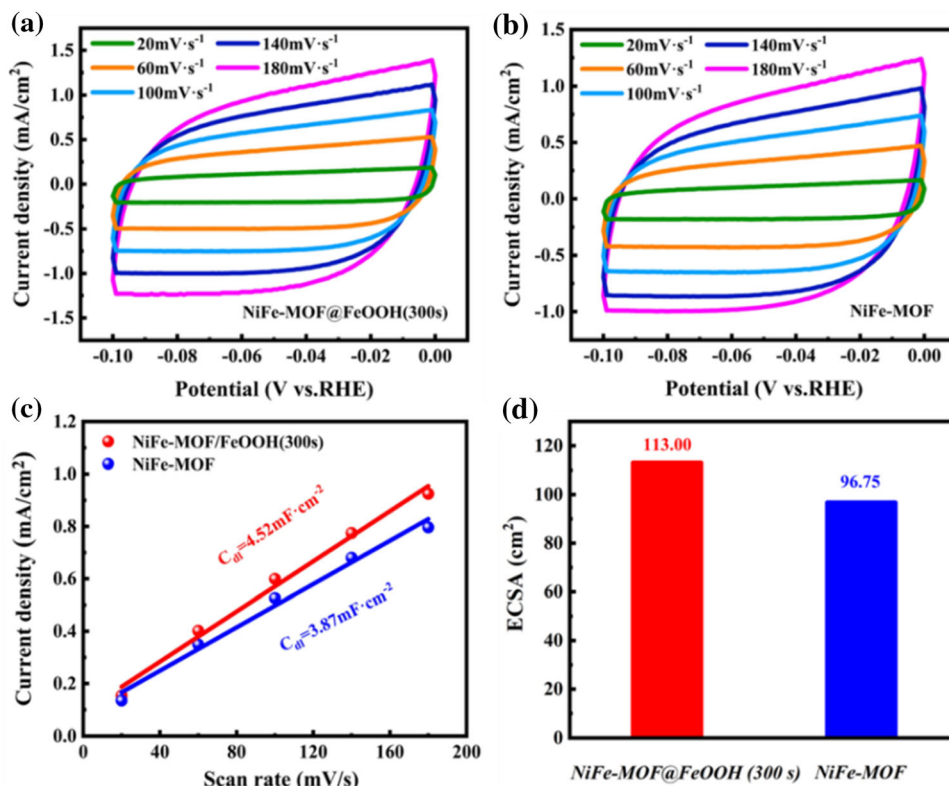


**Figure 7** **a** LSV curve for the HER of NiFe-MOF@FeOOH(300 s). The inset exhibited the corresponding HER performance of FeOOH; **b** The corresponding Tafel plot and **c** EIS impedance diagram; **d** i-t test of NiFe-

MOF@FeOOH(300 s) at 0.137 V vs RHE. The EIS diagrams **e** and LSV curves **f** of NiFe-MOF@FeOOH(300 s) before and after 18 h circles.

**Table 1** Comparison of the electrocatalytic properties of the NiFe-MOF@FeOOH(300 s) electrode in this work with other related materials

Electrocatalysts	OER	HER	References
NiFe-MOF@FeOOH (300 s)	303( $\eta$ 40)	137( $\eta$ 10)	Our work
NiCo-300	320( $\eta$ 10)	156( $\eta$ 10)	[65]
NiFe@C	274( $\eta$ 10)	195( $\eta$ 10)	[66]
NG-NiFe@MoC <sub>2</sub> -2	320( $\eta$ 10)	150( $\eta$ 10)	[67]
FeNiP/NCH	250( $\eta$ 10)	216( $\eta$ 10)	[68]
NiCoFeP/C	270( $\eta$ 10)	149( $\eta$ 10)	[69]
Ni <sub>3</sub> S <sub>2</sub> @MoS <sub>2</sub> /FeOOH	234( $\eta$ 10)	95( $\eta$ 10)	[70]
Cu <sub>3</sub> P@NiFe-MOF	229( $\eta$ 10)	175( $\eta$ 10)	[71]
N-FeP	440( $\eta$ 100)	226( $\eta$ 10)	[72]
Ni/Co-MOF@CoO/NF	290( $\eta$ 10)	139( $\eta$ 10)	[73]
CoP-NC@NFP	270( $\eta$ 10)	162( $\eta$ 10)	[74]

electrochemical stability of NiFe-MOF@FeOOH(300 s) as shown in Fig. 7d. Apparently, it exhibited excellent stability for nearly 18 h without obvious decay. Furthermore, the EIS and LSV curves of NiFe-MOF@FeOOH(300 s) catalyst almost overlapped before and after 18 h(as depicted in Fig. 7e and Fig. 7f), which verified the robustness of the composites. Based on obtained results, it can be found that the constructed NiFe-MOF@FeOOH(300 s) expressed both excellent OER and HER performance, which was also superior than other related materials as exhibited in the Table 1. There was no question that an excellent kind of dual-functional electrocatalyst based on NiFe-MOF@FeOOH had been synthesized.

The prominent performance of the prepared NiFe-MOF@FeOOH(300 s) can be possibly attributed to the following factors: (1) In alkaline media, the abundant FeOOH nanoparticles are closely attached to NiFe-MOF nanosheets to form stable heterojunction structure which can ensure strong synergistic effect and efficiently promote the electron flow, showing improved electrical conductivity. (2) As displayed in Figs. 5e and 6, the formed novel three-dimensional hierarchical structure of NiFe-MOF@FeOOH(300 s) depicted larger electrochemical surface area and could provide more active sites for electrochemical reactions, thus boosting the overall performance. (3) Moreover, the adopted FeOOH was proved to lower and regulate the energy barrier of Ni<sup>2+</sup>/Ni<sup>3+</sup> conversion. The presence of Ni<sup>3+</sup> species could act as the active centers of catalytic reaction, thus promoting the OER process.

## Conclusion

In summary, extraordinary types of dual-function catalyst NiFe-MOF@FeOOH were successfully fabricated by solvothermal route and subsequent electrodeposition strategy. When the deposition time was set as 300 s, NiFe-MOF@FeOOH(300 s) displayed the most fascinating HER and OER performance with a small overpotential of 137 mV at 10 mA cm<sup>-2</sup> and 303 mV at 40 mA cm<sup>-2</sup>, respectively. Meanwhile, it can be verified that the optimal sample NiFe-MOF@FeOOH(300 s) exhibited higher kinetic rate, superior conductivity and durability than that of NiFe-MOF, NiFe-MOF@FeOOH(100 s) and NiFe-MOF@FeOOH(500 s), attributing to the strong synergistic effects between NiFe-MOF and FeOOH. Electrochemical tests also revealed that the decorated FeOOH nanospheres can promote the transformation of Ni<sup>2+</sup>/Ni<sup>3+</sup> and advance electron transmission to enhance the electrical conductivity. Moreover, the constructed 3D hierarchical structure was believed to provide numerous active sites and guarantee sufficient infiltration of the electrolyte. As demonstrated by ECSA calculation, the electrochemical specific surface area of NiFe-MOF@FeOOH(300 s) can reach up to 113.00 cm<sup>2</sup>, thus depicting the remarkable electrocatalytic performance. All in all, this work renders a promising type of dual-function MOF-based electrocatalyst for application in energy conversion.

## Acknowledgements

This work was financially supported by the National Natural Science Foundation of China (21405105), the

Shanghai Natural Science Foundation (14ZR1429300), State Key Laboratory of Green Catalysis of Sichuan Institutes of Higher Education (LZJ1703).

## References

- [1] Liang Q, Chen J, Wang F et al (2020) Transition metal-based metal-organic frameworks for oxygen evolution reaction. *Coord Chem Rev* 424:213488. <https://doi.org/10.1016/j.ccr.2020.213488>
- [2] Wang Y-C, Liu X-Y, Wang X-X et al (2021) Metal-organic frameworks based photocatalysts: Architecture strategies for efficient solar energy conversion. *Chem Eng J* 419:129459. <https://doi.org/10.1016/j.cej.2021.129459>
- [3] Du X, Huang J, Zhang J et al (2019) Modulating electronic structures of inorganic nanomaterials for efficient electrocatalytic water splitting. *Angew Chem Int Edit* 58(14):4484–4502. <https://doi.org/10.1002/anie.201810104>
- [4] You B, Sum Y (2018) Innovative strategies for electrocatalytic water splitting. *Acc Chem Res* 51(7):1571–1580. <https://doi.org/10.1021/acs.accounts.8b00002>
- [5] Sun Y, Zang Y, Tian W et al (2022) Plasma-induced large-area N, Pt-doping and phase engineering of MoS<sub>2</sub> nanosheets for alkaline hydrogen evolution. *Energy Environ Sci* 15(3):1201–1210. <https://doi.org/10.1039/d1ee03825g>
- [6] Nam Y, Kim D, Chu J et al (2022) Highly efficient and stable iridium oxygen evolution reaction electrocatalysts based on porous nickel nanotube template enabling tandem devices with solar-to-hydrogen conversion efficiency exceeding 10%. *Adv Sci* 9(9):2104938. <https://doi.org/10.1002/advs.202104938>
- [7] Chen X, Wan J, Wang J et al (2021) Atomically dispersed ruthenium on nickel hydroxide ultrathin nanoribbons for highly efficient hydrogen evolution reaction in alkaline media. *Adv Mater* 33(44):2104764. <https://doi.org/10.1002/adma.202104764>
- [8] Liu J, Zhang H, Qiu M et al (2020) A review of non-precious metal single atom confined nanomaterials in different structural dimensions(1D–3D) as highly active oxygen redox reaction electrocatalysts. *J Mater Chem A* 8(5):2222–2245. <https://doi.org/10.1039/c9ta11852g>
- [9] Chen Z, Duan X, Wei W et al (2020) Iridium-based nanomaterials for electrochemical water splitting. *Nano Energy* 78:105270. <https://doi.org/10.1016/j.nanoen.2020.105270>
- [10] Zhang Z, Zhou J, Wei H et al (2020) Construction of hierarchical NiFe-LDH/FeCoS<sub>2</sub>/CFC composites as efficient bifunctional electrocatalysts for hydrogen and oxygen evolution reaction. *J Mater Sci* 55(35):16625–16640. <https://doi.org/10.1007/s10853-020-05182-5>
- [11] Jiang D, Ma W, Yang R et al (2020) Nickel–manganese bimetallic phosphides porous nanosheet arrays as highly active bifunctional hydrogen and oxygen evolution electrocatalysts for overall water splitting. *Electrochim Acta* 329:135121. <https://doi.org/10.1016/j.electacta.2019.135121>
- [12] Si F, Tang C, Gao Q et al (2020) Bifunctional CdS@Co<sub>9</sub>S<sub>8</sub>/Ni<sub>3</sub>S<sub>2</sub> catalyst for efficient electrocatalytic and photo-assisted electrocatalytic overall water splitting. *J Mater Chem A* 8(6):3083–3096. <https://doi.org/10.1039/c9ta11921c>
- [13] Chen J, Ren B, Cui H et al (2020) Constructing pure phase tungsten-based bimetallic carbide nanosheet as an efficient bifunctional electrocatalyst for overall water splitting. *Small* 16(23):1907556. <https://doi.org/10.1002/sml.201907556>
- [14] Guo P, Wu J, Li X-B et al (2018) A highly stable bifunctional catalyst based on 3D Co(OH)<sub>2</sub>@NCNTs@NF towards overall water-splitting. *Nano Energy* 47:96–104. <https://doi.org/10.1016/j.nanoen.2018.02.032>
- [15] Lin Y, Wan H, Wu D et al (2020) Metal–organic framework hexagonal nanoplates: bottom-up synthesis, topotactic transformation, and efficient oxygen evolution reaction. *J Am Chem Soc* 142(16):7317–7321. <https://doi.org/10.1021/jacs.0c01916>
- [16] Wang C, Kim J, Tang J et al (2020) New strategies for novel mof-derived carbon materials based on nanoarchitectures. *Chem* 6(1):19–40. <https://doi.org/10.1016/j.chempr.2019.09.005>
- [17] Ge X, Li Z, Yin L (2017) Metal-organic frameworks derived porous core/shell CoP@C polyhedrons anchored on 3D reduced graphene oxide networks as anode for sodium-ion battery. *Nano Energy* 32:117–124. <https://doi.org/10.1016/j.nanoen.2016.11.055>
- [18] Jia Y, Xu Z, Li L et al (2022) Formation of NiFe-MOF nanosheets on Fe foam to achieve advanced electrocatalytic oxygen evolution. *Dalton Trans* 51(13):5053–5060. <https://doi.org/10.1039/d2dt00127f>
- [19] Li CF, Xie LJ, Zhao JW et al (2022) Interfacial Fe–O–Ni–O–Fe bonding regulates the active ni sites of Ni-MOFs via Iron doping and decorating with FeOOH for super-efficient oxygen evolution. *Angew Chem Int Edit* 61(17):e202116934. <https://doi.org/10.1002/anie.202116934>
- [20] Sun F, Wang G, Ding Y et al (2018) NiFe-based metal–organic framework nanosheets directly supported on nickel foam acting as robust electrodes for electrochemical oxygen evolution reaction. *Adv Energy Mater* 8(21):1800584. <https://doi.org/10.1002/aenm.201800584>
- [21] Xing J, Guo K, Zou Z et al (2018) In situ growth of well-ordered NiFe-MOF-74 on Ni foam by Fe<sup>2+</sup> induction as an efficient and stable electrocatalyst for water oxidation. *ChemComm* 54(51):7046–7049. <https://doi.org/10.1039/c8cc03112f>



- [22] Wen Y, Chen P, Wang L et al (2021) Stabilizing highly active Ru sites by suppressing lattice oxygen participation in acidic water oxidation. *J Am Chem Soc* 143(17):6482–6490. <https://doi.org/10.1021/jacs.1c00384>
- [23] Zhao J, Zhang X, Liu M et al (2019) Metal–organic-framework-derived porous 3D heterogeneous NiFe<sub>x</sub>/NiFe<sub>2</sub>O<sub>4</sub>@NC nanoflowers as highly stable and efficient electrocatalysts for the oxygen-evolution reaction. *J Mater Chem A* 7(37):21338–21348. <https://doi.org/10.1039/c9ta08077e>
- [24] Wang Y, Liu B, Shen X et al (2021) Engineering the activity and stability of MOF-nanocomposites for efficient water oxidation. *Adv Energy Mater* 11(16):2003759. <https://doi.org/10.1002/aenm.202003759>
- [25] Ying M, Tang R, Yang W et al (2021) Tailoring electronegativity of bimetallic Ni/Fe metal–organic framework nanosheets for electrocatalytic water oxidation. *ACS Appl Nano Mater* 4(2):1967–1975. <https://doi.org/10.1021/acsnano.0c03310>
- [26] Chen W, Zhu X, Zhang Y et al (2021) Bimetal–organic frameworks from in situ-activated NiFe foam for highly efficient water splitting. *ACS Sustain Chem Eng* 9(4):1826–1836. <https://doi.org/10.1021/acssuschemeng.0c08147>
- [27] Wang Y, Tang W, Li X et al (2021) Improving the electrocatalytic activity of NiFe bimetal–organic framework toward oxygen evolution reaction by Zr doping. *Electrochim Acta* 381:138292. <https://doi.org/10.1016/j.electacta.2021.138292>
- [28] Wu S, Shen X, Zhu G et al (2017) Metal organic framework derived NiFe@N-doped graphene microtube composites for hydrogen evolution catalyst. *Carbon* 116:68–76. <https://doi.org/10.1016/j.carbon.2017.01.085>
- [29] Wu M, Zhang Y, Zhang R et al. (2022) Highly active oxygen evolution reaction electrocatalyst based on defective-CeO<sub>2</sub>-x decorated MOF(Ni/Fe). *Electrochim. Acta* 403:139630. Doi: <https://doi.org/10.1016/j.electacta.2021.139630>.
- [30] Qiu T, Liang Z, Guo W et al (2020) Metal–organic framework-based materials for energy conversion and storage. *ACS Energy Lett* 5(2):520–532. <https://doi.org/10.1021/acseenergylett.9b02625>
- [31] Li X, Ma D-D, Cao C et al (2019) Inlaying ultrathin bimetallic MOF nanosheets into 3d ordered macroporous hydroxide for superior electrocatalytic oxygen evolution. *Small* 15(35):1902218. <https://doi.org/10.1002/sml.201902218>
- [32] Abazari R, Sanati S, Morsali A (2022) Mixed metal Fe<sub>2</sub>Ni MIL-88B metal–organic frameworks decorated on reduced graphene oxide as a robust and highly efficient electrocatalyst for alkaline water oxidation. *Inorg Chem* 61(8):3396–3405. <https://doi.org/10.1021/acs.inorgchem.1c03216>
- [33] An H, Hu Y, Song N et al (2022) Two-dimensional heterostructures built from ultrathin CeO<sub>2</sub> nanosheet surface-coordinated and confined metal–organic frameworks with enhanced stability and catalytic performance. *Chem Sci* 13(10):3035–3044. <https://doi.org/10.1039/d2sc00308b>
- [34] Zhang H, Li W, Feng X et al (2021) Interfacial FeOOH/CoO nanowires array improves electrocatalytic water splitting. *J Solid State Chem* 298:122156. <https://doi.org/10.1016/j.jssc.2021.122156>
- [35] Gao J, Ma H, Zhang L et al (2022) Interface engineering of Ni<sub>3</sub>Se<sub>2</sub>@FeOOH heterostructure nanoforests for highly-efficient overall water splitting. *J Alloys Compd* 893:162244. <https://doi.org/10.1016/j.jssc.2021.122156>
- [36] Li M, Tao L, Xiao X et al (2018) Core-shell structured NiCo<sub>2</sub>O<sub>4</sub>@FeOOH nanowire arrays as bifunctional electrocatalysts for efficient overall water splitting. *ChemCatChem* 10(18):4119–4125. <https://doi.org/10.1002/cctc.201800606>
- [37] Chen J, Zheng F, Zhang S-J et al (2018) Interfacial Interaction between FeOOH and Ni–Fe LDH to modulate the local electronic structure for enhanced OER electrocatalysis. *ACS Catal* 8(12):11342–11351. <https://doi.org/10.1021/acscatal.8b03489>
- [38] Liang Y, Wang J, Liu D et al (2021) Ultrafast Fenton-like reaction route to FeOOH/NiFe-LDH heterojunction electrode for efficient oxygen evolution reaction. *J Mater Chem A* 9(38):21785–21791. <https://doi.org/10.1039/d1ta05136a>
- [39] Yao J, Ji Y, Pei L et al (2022) Amorphous FeOOH nanoparticles decorated on defect-rich porous Ni MOF nanosheet based hierarchical architectures toward superior OER performance. *New J Chem* 46(20):9650–9657. <https://doi.org/10.1039/d2nj01385a>
- [40] Wang Y, Liu B, Shen X et al (2021) Engineering the activity and stability of MOF-nanocomposites for efficient water oxidation. *Adv Energy Mater* 11(16):2003759. <https://doi.org/10.1002/aenm.202003759>
- [41] Thangavel P, Ha M, Kumaraguru S et al (2020) Graphene-nanoplatelets-supported NiFe-MOF: high-efficiency and ultra-stable oxygen electrodes for sustained alkaline anion exchange membrane water electrolysis. *Energy Environ Sci* 13(10):3447–3458. <https://doi.org/10.1039/d0ee00877j>
- [42] Zhao T, Cheng C, Wang D et al (2021) Preparation of a bimetallic NiFe-MOF on nickel foam as a highly efficient electrocatalyst for oxygen evolution reaction. *ChemistrySelect* 6(6):1320–1327. <https://doi.org/10.1002/slct.202004504>
- [43] Zhang W-D, Yu H, Li T et al (2020) Hierarchical trimetallic layered double hydroxide nanosheets derived from 2D metal-organic frameworks for enhanced oxygen evolution reaction. *Appl Catal B* 264:118532. <https://doi.org/10.1016/j.apcatb.2019.118532>

- [44] Chen X, Wang Q, Cheng Y, et al. (2022) S-doping triggers redox reactivities of both iron and lattice oxygen in FeOOH for low-cost and high-performance water oxidation. *Adv Funct Mater*, p 2112674. Doi: <https://doi.org/10.1002/adfm.202112674>.
- [45] Meng X, Han J, Lu L et al (2019) Fe<sup>(2+)</sup>-doped layered double(Ni, Fe) hydroxides as efficient electrocatalysts for water splitting and self-powered electrochemical systems. *Small* 15(41):e1902551. <https://doi.org/10.1002/sml.201902551>
- [46] Qiu C, He S, Wang Y et al (2020) Interfacial engineering FeOOH/CoO nanoneedle array for efficient overall water splitting driven by solar energy. *Chem Eur J* 26(18):4120–4127. <https://doi.org/10.1002/adfm.202112674>
- [47] Luo P, Li S, Zhao Y et al (2019) In-situ Growth of a bimetallic cobalt-nickel organic framework on iron foam: achieving the electron modification on a robust self-supported oxygen evolution electrode. *ChemCatChem* 11(24):6061–6069. <https://doi.org/10.1002/adfm.202112674>
- [48] Jiang K, Liu W, Lai W et al (2021) NiFe layered double hydroxide/FeOOH heterostructure nanosheets as an efficient and durable bifunctional electrocatalyst for overall seawater splitting. *Inorg Chem* 60(22):17371–17378. <https://doi.org/10.1002/cctc.201900972>
- [49] Li W, Li F, Yang H et al (2019) A bio-inspired coordination polymer as outstanding water oxidation catalyst via second coordination sphere engineering. *Nat Commun* 10(1):5074. <https://doi.org/10.1038/s41467-019-13052-1>
- [50] Ma P, Luo S, Luo Y et al (2020) Vertically aligned FeOOH nanosheet arrays on alkali-treated nickel foam as highly efficient electrocatalyst for oxygen evolution reaction. *J Colloid Interface Sci* 574:241–250. <https://doi.org/10.1016/j.jcis.2020.04.058>
- [51] Hao S, Chen L, Yu C et al (2019) NiCoMo hydroxide nanosheet arrays synthesized via chloride corrosion for overall water splitting. *ACS Energy Lett* 4(4):952–959. <https://doi.org/10.1021/acscenergylett.9b00333>
- [52] Zhang Y, Cheng C-Q, Kuai C-G et al (2020) Unveiling the critical role of the Mn dopant in a NiFe(OH)<sub>2</sub> catalyst for water oxidation. *J Mater Chem A* 8(34):17471–17476. <https://doi.org/10.1039/d0ta06353c>
- [53] Qiao X, Kang H, Li Y et al (2022) Novel FeNi-based nanowires network catalyst involving hydrophilic channel for oxygen evolution reaction. *Small* 18(10):e2106378. <https://doi.org/10.1002/sml.202106378>
- [54] Yu J, Wang J, Long X et al (2021) Formation of FeOOH nanosheets induces substitutional doping of CeO<sub>2-x</sub> with high-valence Ni for efficient water oxidation. *Adv Energy Mater* 11(4):2002731. <https://doi.org/10.1002/aenm.202002731>
- [55] Li N, Bediako DK, Hadt RG et al (2017) Influence of iron doping on tetravalent nickel content in catalytic oxygen evolving films. *Proc Natl Acad Sci USA* 114(7):1486–1491. <https://doi.org/10.1073/pnas.1620787114>
- [56] Lu X, Zhao C (2015) Electrodeposition of hierarchically structured three-dimensional nickel–iron electrodes for efficient oxygen evolution at high current densities. *Nat Commun* 6(1):6616. <https://doi.org/10.1038/ncomms7616>
- [57] Zhao Y, Luo M, Chu S et al (2019) 3D nanoporous iridium-based alloy microwires for efficient oxygen evolution in acidic media. *Nano Energy* 59:146–153. <https://doi.org/10.1016/j.nanoen.2019.02.020>
- [58] Tan S, Ouyang W, Ji Y et al (2021) Carbon wrapped bimetallic NiCo nanospheres toward excellent HER and OER performance. *J Alloys Compd* 889:161528. <https://doi.org/10.1016/j.jallcom.2021.161528>
- [59] Tan S, Ji Y, Ren F et al (2022) Improved energy conversion and storage performance enabled by hierarchical zigzag-like P-doped CuCo<sub>2</sub>O<sub>4</sub> nanosheets based 3D electrode materials. *Int J Hydrog Energy* 47(15):9248–9260. <https://doi.org/10.1016/j.ijhydene.2021.12.268>
- [60] Chen C, Suo N, Han X et al (2021) Tuning the morphology and electron structure of metal-organic framework-74 as bifunctional electrocatalyst for OER and HER using bimetallic collaboration strategy. *J Alloys Compd* 865:158795. <https://doi.org/10.1016/j.jallcom.2021.158795>
- [61] Li X, Ma DD, Cao C et al (2019) Inlaying ultrathin bimetallic MOF nanosheets into 3D ordered macroporous hydroxide for superior electrocatalytic oxygen evolution. *Small* 15(35):e1902218. <https://doi.org/10.1002/sml.201902218>
- [62] Yaqoob L, Noor T, Iqbal N et al (2021) Electrochemical synergies of Fe–Ni bimetallic MOF CNTs catalyst for OER in water splitting. *J Alloys Compd* 850:156583. <https://doi.org/10.1016/j.jallcom.2020.156583>
- [63] Lin Y, Wang H, Peng C-K, et al. (2021) Co-induced electronic optimization of hierarchical NiFe LDH for oxygen evolution. *Small* 16(38):2002426. Doi: <https://doi.org/10.1002/sml.202002426>.
- [64] Tian Y, Zhang Y, Huang A et al (2020) Nanostructured Ni<sub>2</sub>SeS on Porous-carbon skeletons as highly efficient electrocatalyst for hydrogen evolution in acidic medium. *Inorg Chem* 59(9):6018–6025. <https://doi.org/10.1021/acs.inorgchem.0c00012>
- [65] Sun T, Cao J, Dong J et al (2017) Ordered mesoporous NiCo alloys for highly efficient electrocatalytic hydrogen evolution reaction. *Int J Hydrog Energy* 42(10):6637–6645. <https://doi.org/10.1016/j.ijhydene.2017.01.071>
- [66] Park S-W, Kim I, Oh S-I et al (2018) Carbon-encapsulated NiFe nanoparticles as a bifunctional electrocatalyst for high-

- efficiency overall water splitting. *J Catal* 366:266–274. <https://doi.org/10.1016/j.jcat.2018.08.016>
- [67] Hu Q, Liu X, Zhu B et al (2018) Crafting MoC<sub>2</sub>-doped bimetallic alloy nanoparticles encapsulated within N-doped graphene as roust bifunctional electrocatalysts for overall water splitting. *Nano Energy* 50:212–219. <https://doi.org/10.1002/adfm.202112674>
- [68] Wei Y-S, Zhang M, Kitta M et al (2019) A single-crystal open-capsule metal–organic framework. *J Am Chem Soc* 141(19):7906–7916. <https://doi.org/10.1021/jacs.9b02417>
- [69] Wei X, Zhang Y, He H et al (2019) Carbon-incorporated porous honeycomb NiCoFe phosphide nanospheres derived from a MOF precursor for overall water splitting. *Chem-Comm* 55(73):10896–10899. <https://doi.org/10.1039/c9cc05225a>
- [70] Zheng M, Guo K, Jiang W-J et al (2019) When MoS<sub>2</sub> meets FeOOH: A “one-stone-two-birds” heterostructure as a bifunctional electrocatalyst for efficient alkaline water splitting. *Appl Catal B* 244:1004–1012. <https://doi.org/10.1016/j.apcatb.2018.12.019>
- [71] Li E, Mou Q, Xu Z et al (2022) A Cu<sub>3</sub>P@NiFe-MOF hybrid as an efficient electrocatalyst for hydrogen and oxygen evolution reactions. *Catal Letters*. <https://doi.org/10.1007/s10562-021-03865-5>
- [72] Yang M, Xie J-Y, Lin Z-Y et al (2020) N-doped FeP nanorods derived from Fe-MOFs as bifunctional electrocatalysts for overall water splitting. *Appl Surf Sci* 507:145096. <https://doi.org/10.1016/j.apsusc.2019.145096>
- [73] Van Phuc T, Jana J, Ravi N et al (2022) Highly active Ni/Co-metal organic framework bifunctional electrocatalyst for water splitting reaction. *Int J Hydrog Energy* 47(54):22787–22795. <https://doi.org/10.1016/j.ijhydene.2022.05.097>
- [74] Vijayakumar E, Ramakrishnan S, Sathiskumar C et al (2022) MOF-derived CoP-nitrogen-doped carbon@NiFeP nanoflakes as an efficient and durable electrocatalyst with multiple catalytically active sites for OER, HER, ORR and rechargeable zinc-air batteries. *Chem Eng J* 428:131115. <https://doi.org/10.1016/j.cej.2021.131115>

**Publisher’s Note** Springer Nature remains neutral with regard to jurisdictional claims in published maps and institutional affiliations.

Springer Nature or its licensor holds exclusive rights to this article under a publishing agreement with the author(s) or other rightsholder(s); author self-archiving of the accepted manuscript version of this article is solely governed by the terms of such publishing agreement and applicable law.